九州大学学術情報リポジトリ
Kyushu University Institutional Repository

# Antitumor activity of tumor-infiltrating neutrophils revealed by a syngeneic mouse model of cholangiocarcinoma

須賀原, 修

https://hdl.handle.net/2324/7443307

出版情報：Kyushu University, 2025, 博士（医学）, 課程博士
バージョン：
権利関係：© 2025 The Author(s).

KYUSHU UNIVERSITY

Check for updates

*Cancer Science*

WILEY

Cancer Science

ORIGINAL ARTICLE OPEN ACCESS

# Antitumor Activity of Tumor-Infiltrating Neutrophils Revealed by a Syngeneic Mouse Model of Cholangiocarcinoma

Osamu Sugahara[1,2] | Daisuke Koga[2] | Takeru Oka[2] | Shigeaki Sugiyama[2] | Reona Wada[2] | Tsunaki Higa[1,2] | Keiichi I. Nakayama[1,2]

[1]Anticancer Strategies Laboratory, Advanced Research Initiative, Institute of Science Tokyo, Tokyo, Japan | [2]Department of Molecular and Cellular Biology, Medical Institute of Bioregulation, Kyushu University, Fukuoka, Japan

**Correspondence:** Tsunaki Higa (higa.tsunaki@tmd.ac.jp) | Keiichi I. Nakayama (nakayama.keiichi@tmd.ac.jp)

**Received:** 15 February 2025 | **Revised:** 3 June 2025 | **Accepted:** 12 June 2025

**Funding:** This work was supported by Japan Agency for Medical Research and Development, JP23ck0106802/JP23ama221119. Japan Society for the Promotion of Science, JP23H00378.

**Keywords:** cholangiocarcinoma | granulocyte colony-stimulating factor (G-CSF) | neutrophil | organoid | tumor microenvironment

## ABSTRACT

The tumor immune microenvironment plays a key role in the regulation of cancer progression. Recent studies have suggested a relation between diverse tumor genotypes and tumor immune microenvironment phenotypes for cholangiocarcinoma (CCA). However, the contribution of tumor-infiltrating immune cells to CCA progression has remained unclear, underscoring the need for genetically defined CCA models in immunocompetent mice. We here aimed to generate genetically engineered and transplantable CCA organoids from C57BL/6 mice and to investigate the role of tumor-infiltrating immune cells in CCA progression with this model. CCA organoids were generated ex vivo with the use of the CRISPR/Cas9 system. Orthotopic transplantation of CCA organoids harboring mutations in *Smad4*, *Trp53*, and *Kras* into wild-type C57BL/6 mice resulted in tumor formation accompanied by distant metastasis. Selective depletion of immune cell types in the tumor-bearing mice revealed an antitumor action of tumor-infiltrating neutrophils (TINs) that was mediated by direct killing of cancer cells through the production of reactive oxygen species. Furthermore, administration of recombinant human granulocyte colony-stimulating factor (rhG-CSF) increased the number and cytotoxicity of TINs, suppressed tumor growth, and prolonged the survival of tumor-bearing mice. Finally, combination treatment with rhG-CSF and standard chemotherapy resulted in a synergistic attenuation of tumor growth. Our study therefore provides a syngeneic and genetically defined mouse model of CCA and highlights the therapeutic potential of targeting TINs with rhG-CSF.

**Abbreviations:** 7AAD, 7-aminoactinomycin D; CCA, cholangiocarcinoma; CCR2, C-C chemokine receptor type 2; CRISPR, clustered regularly interspaced short palindromic repeats; DAPI, 4′,6-diamidino-2-phenylindole; DEG, differentially expressed gene; EGF, epidermal growth factor; FACS, fluorescence-activated cell sorting; FGF10, fibroblast growth factor 10; GO, gene ontology; HGF, hepatocyte growth factor; Krt19, cytokeratin 19; PAM, protospacer adjacent motif; PBS, phosphate-buffered saline; rhG-CSF, recombinant human granulocyte colony-stimulating factor; ROS, reactive oxygen species; scRNA-seq, single-cell RNA-sequencing; sgRNA, single guide RNA; SOD, superoxide dismutase; TGF-β, transforming growth factor–β; TIN, tumor-infiltrating neutrophil; Treg, regulatory T cell; *t*-SNE, *t*-distributed stochastic neighbor embedding; WT, wild-type; αSMA, α-smooth muscle actin.

This is an open access article under the terms of the Creative Commons Attribution-NonCommercial-NoDerivs License, which permits use and distribution in any medium, provided the original work is properly cited, the use is non-commercial and no modifications or adaptations are made.

© 2025 The Author(s). *Cancer Science* published by John Wiley & Sons Australia, Ltd on behalf of Japanese Cancer Association.

## 1 | Introduction

Cholangiocarcinoma (CCA) is a highly malignant tumor of the biliary tract whose incidence and mortality rates are both increasing [1, 2]. Although surgical resection remains the primary curative treatment for CCA, most patients are diagnosed with advanced disease. Systemic chemotherapy has limited efficacy in such cases, highlighting the need for more effective treatments. Given that the tumor microenvironment for CCA contains a greater abundance of immune cells compared with normal tissue, and that the extent of the infiltration of these cells is associated with patient life expectancy [3], tumor-infiltrating immune cells have been considered a promising therapeutic target. However, recent genetic studies have revealed diverse genetic profiles of CCA [4–8], with the corresponding tumors differing in their sensitivity to immune checkpoint inhibition [9]. These findings suggest that the nature of the tumor immune microenvironment differs among CCA genotypes, underscoring the need for genetically defined models to study the interplay between cancer cells and stromal cells in CCA.

Among the most frequent genetic aberrations in CCA are constitutively activating mutations of *KRAS* and loss-of-function mutations of *TP53* and *SMAD4* [4–8], with these mutations often occurring in the same tumors [4, 7]. Of these three genes, inactivation of *Smad4* uniquely promotes biliary proliferation in response to injury [10]. Genetic alterations of *SMAD4*, *TP53*, and *KRAS* have been detected in low-grade dysplasia, high-grade dysplasia, and CCA, respectively [11], suggestive of a mutational sequence during CCA carcinogenesis. In addition, these various mutations are associated with shorter overall survival and a poor therapeutic response to conventional chemotherapy as well as to immune checkpoint blockade in CCA patients [7, 12]. Despite the clinical evidence implicating *SMAD4*, *TP53*, and *KRAS* mutations in the malignancy of CCA, no genetically defined CCA models that recapitulate the sequential acquisition of these mutations have been developed to date.

The tumor immune microenvironment plays a key role in the regulation of cancer progression, with anticancer immunity being considered a promising therapeutic target. Although most studies of immunotherapy to date have focused on T lymphocytes and macrophages, recent evidence has suggested the importance of tumor-infiltrating neutrophils (TINs) [13]. Neutrophils are the most abundant myeloid cells in human blood, and they constitute a heterogeneous cell population in both healthy and diseased states [14]. They have been shown to perform multifaceted functions in a variety of cancer types [15], with protumoral activities having been demonstrated for these cells in immunodeficient mouse models of CCA [16–18]. Although these findings indicate that TINs might act as a tumor-supportive cell population in CCA, their precise functions in the setting of a genetically defined and immunocompetent CCA microenvironment have remained largely uncharacterized.

Organoids are miniaturized, self-organizing, three-dimensional tissue culture systems that faithfully reproduce various biological aspects of corresponding organs, including gene expression, tissue structure, heterogeneity of cellular components, and stem cell-based hierarchy [19]. Cancer organoids can be established not only from tumor samples but also by CRISPR (clustered regularly interspaced short palindromic repeats)/Cas9-mediated stepwise mutagenesis in normal tissue organoids [20, 21], providing a powerful tool for the study of carcinogenesis. Mice transplanted with cancer organoids provide a time-saving and readily repeatable in vivo experimental platform, compared with spontaneous tumors that develop in genetically engineered mouse models and often require multigenerational cross-breeding. Much effort has been expended to establish patient-derived cancer organoids, which have been shown to retain various functional and pathological aspects of tumors and which therefore provide a more reliable human disease model in comparison with conventional cell lines [22]. On the contrary, given that human organoids require immunodeficient recipients for xenograft transplantation, the application of human CCA organoids to analysis of the tumor immune microenvironment remains a challenge, highlighting the necessity for a CCA organoid model compatible with transplantation to immunocompetent mice.

We have now generated genetically engineered mouse CCA organoids by sequential introduction of *Smad4*, *Trp53*, and *Kras* mutations into normal liver ductal organoids in vitro. Orthotopic transplantation of these organoids into immunocompetent mice resulted in the formation of invasive and metastatic tumors with features of human CCA. Selective depletion of tumor-infiltrating immune cells in this model revealed that TINs play a protective role in CCA progression through the production of reactive oxygen species (ROS), whereas regulatory T cells (Tregs), monocytes, and M2 macrophages have little effect on tumor growth. The antitumor function of TINs was found to be enhanced by the administration of recombinant human granulocyte colony-stimulating factor (rhG-CSF), resulting in suppression of tumor growth, prolonged mouse survival, and an increased response to chemotherapy. Our findings suggest that enhancement of the antitumoral properties of TINs is a potential novel therapeutic strategy for CCA.

## 2 | Material and Methods

All mice were housed in the specific pathogen-free animal facility at Kyushu University or Institute of Science Tokyo in accordance with institutional guidelines. The experimental procedures included liver organoid culture, genetic manipulation, organoid transplantation, bioluminescence imaging, histological analysis, flow cytometry, killing assays, and single-cell RNA-sequencing (scRNA-seq) analysis. Detailed information can be found in (Data S1).

## 3 | Results

### 3.1 | Generation of Genetically Engineered Mouse CCA Organoids

To model the neoplastic cascade of CCA with mutated *SMAD4*, *TP53*, and *KRAS* genes, we applied the CRISPR/Cas9 genome editing system to cultured mouse organoids (Figure 1A). Normal liver ductal organoids were established from the hepatic hilar region of wild-type (WT) C57BL/6 mice and were maintained



13497006, 2025, 9, Downloaded from https://onlinelibrary.wiley.com/doi/10.1111/cas.70129 by Tokyo Medical & Dental, Wiley Online Library on [06/10/2025]. See the Terms and Conditions (https://onlinelibrary.wiley.com/terms-and-conditions) on Wiley Online Library for rules of use; OA articles are governed by the applicable Creative Commons License

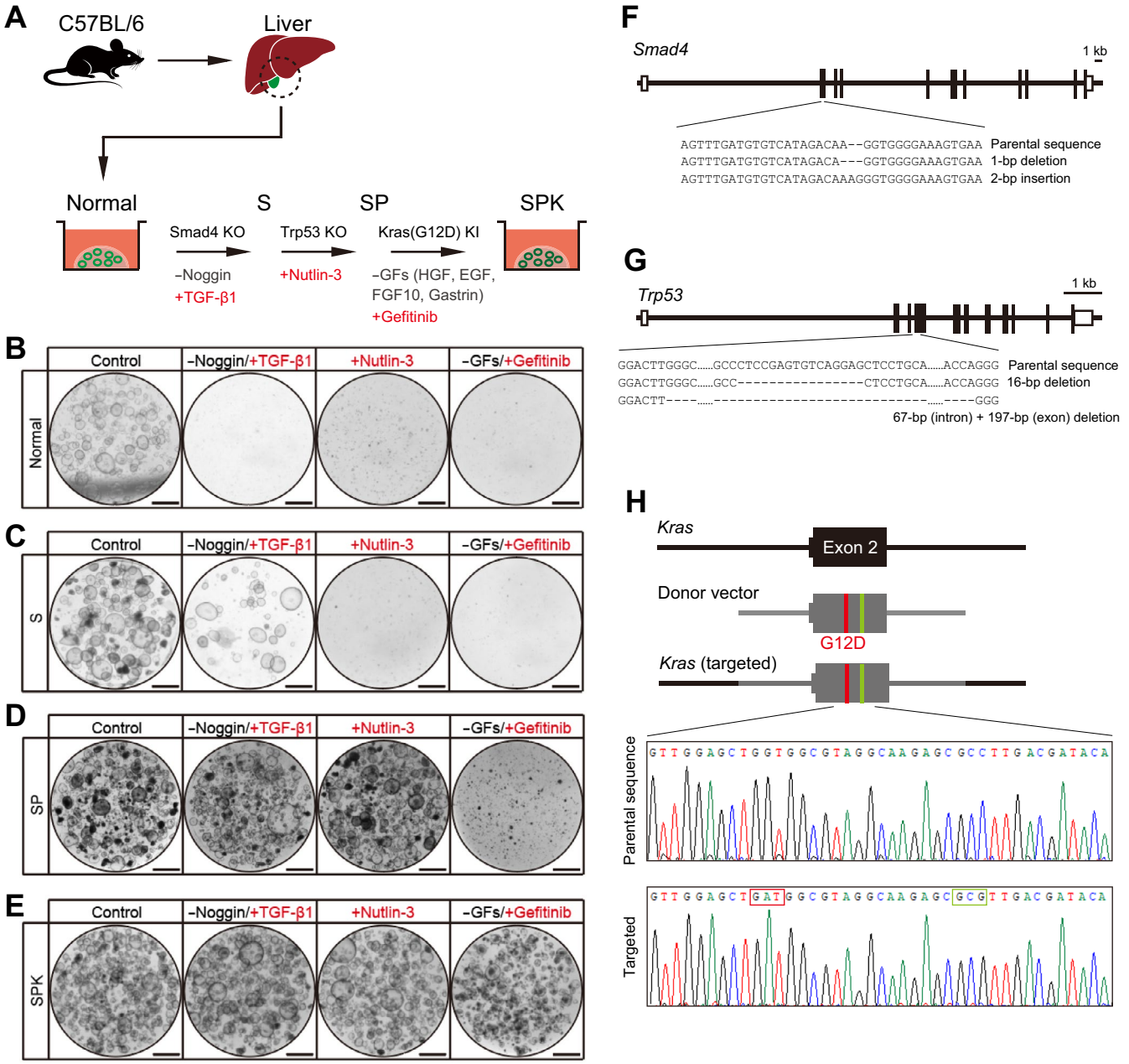



**FIGURE 1** | Ex vivo generation of CCA organoids. (A) Schematic representation for the establishment of normal liver organoids and the sequential introduction of *Smad4* (S), *Trp53* (P), and *Kras* (K) mutations by genome editing with the CRISPR/Cas9 system. KO, knockout; KI, knock-in; GFs, growth factors. (B–E) Growth of normal and genetically engineered liver organoids under the genotype-selective conditions indicated in (A). Scale bars, 1 mm. (F) Sanger sequencing of the *Smad4* locus for liver organoids (S-organoids) grown in medium containing TGF-β1. (G) Sanger sequencing of the *Trp53* locus for liver organoids (SP-organoids) grown in medium containing Nutlin-3. (H) Strategy for modification of the *Kras* locus. A donor vector harboring the G12D mutation of *Kras* (red) and a synonymous mutation in the PAM sequence (green) was introduced into SP-organoids together with the Cas9/sgRNA vector. Successful knock-in was confirmed by Sanger sequencing analysis of SPK-organoids after culture in the selection medium.

in the presence of Noggin (an inhibitor of bone morphogenetic protein [BMP] signaling) as well as epidermal growth factor (EGF), hepatocyte growth factor (HGF), fibroblast growth factor 10 (FGF10), and gastrin (all of which are activators of mitogen-activated protein kinase [MAPK] signaling). The *Smad4* gene was inactivated by transfection of the organoids with a vector encoding the Cas9 protein and a single guide RNA (sgRNA) targeting the *Smad4* coding sequence. Given that transforming growth factor-β (TGF-β) signaling triggers cell cycle arrest and apoptosis by inducing the translocation of Smad complexes to the nucleus [23, 24], only *Smad4*-targeted (S-) organoids were able to expand after the removal of Noggin and addition of TGF-β1 to the culture medium (Figure 1B,C). With a similar strategy, we next targeted the *Trp53* gene in S-organoids. The *Trp53*-targeted (SP-) organoids were selected in the presence of Nutlin-3, which inhibits Mdm2-dependent proteasomal degradation of p53 and thereby induces apoptosis in (p53-expressing) S-organoids (Figure 1C,D). Finally, we introduced a knock-in



13497006, 2025, 9, Downloaded from https://onlinelibrary.wiley.com/doi/10.1111/cas.70129 by Tokyo Medical & Dental, Wiley Online Library on [06/10/2025]. See the Terms and Conditions (https://onlinelibrary.wiley.com/terms-and-conditions) on Wiley Online Library for rules of use; OA articles are governed by the applicable Creative Commons License

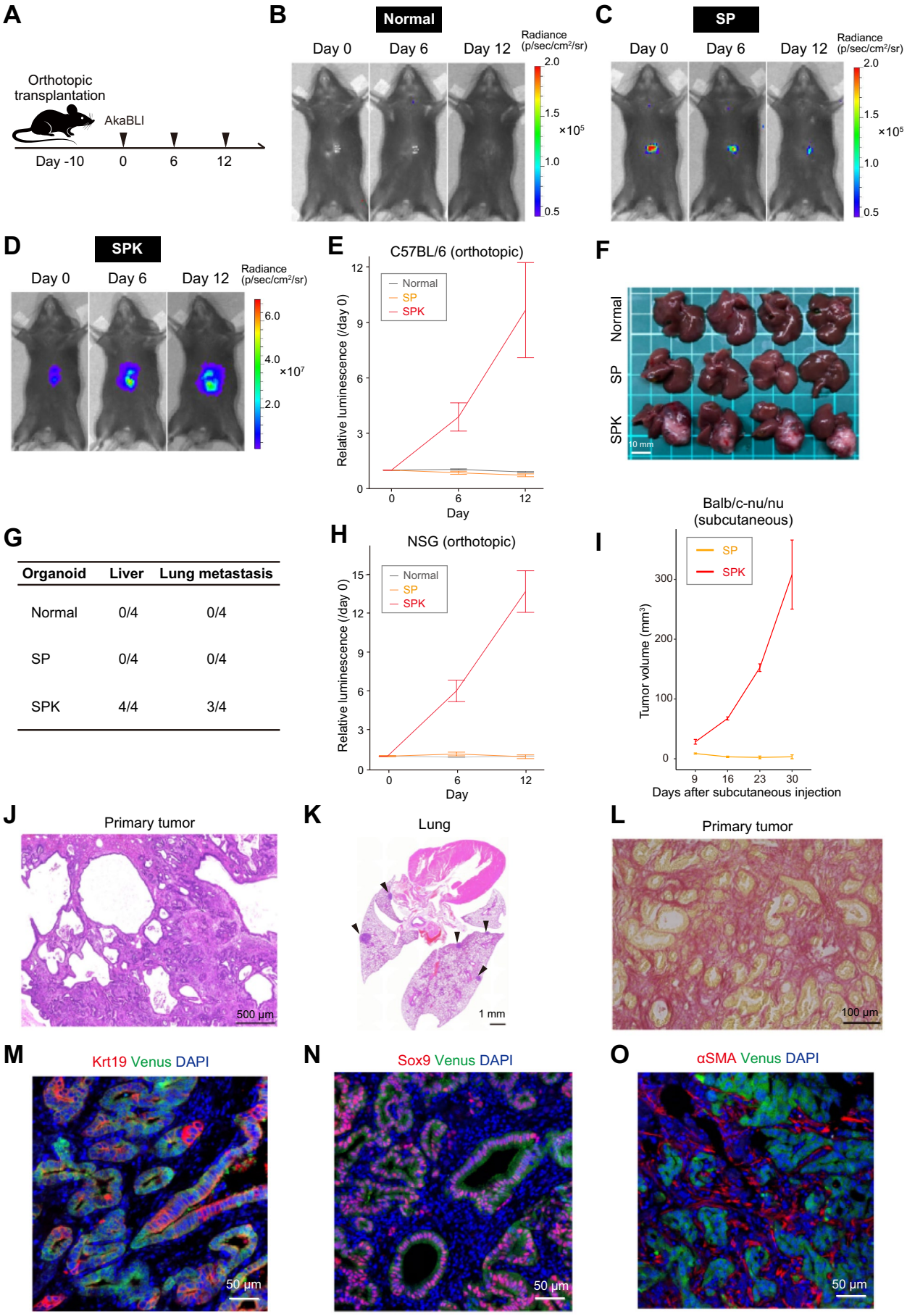



**FIGURE 2** | Legend on next page.



13497006, 2025, 9, Downloaded from https://onlinelibrary.wiley.com/doi/10.1111/cas.70129 by Tokyo Medical & Dental, Wiley Online Library on [06/10/2025]. See the Terms and Conditions (https://onlinelibrary.wiley.com/terms-and-conditions) on Wiley Online Library for rules of use; OA articles are governed by the applicable Creative Commons License

**FIGURE 2** | CRISPR/Cas9-engineered CCA organoids are tumorigenic and metastatic in C57BL/6 mice. (A) Schematic representation of tumorigenicity assays performed for normal, SP-, and SPK-organoids. Organoids expressing retrovirally transduced Venus-Akaluc protein were orthotopically transplanted in C57BL/6 mice on day −10 and analyzed on days 0, 6, and 12. (B–D) Representative Akaluc bioluminescence (AkaBLI) images of orthotopically transplanted normal (B), SP- (C), or SPK- (D) organoids in C57BL/6 mice on days 0, 6, and 12. Radiance units are photons per second per square centimeter per steradian (p/s/cm$^2$/sr). (E) Quantification of bioluminescence of normal, SP-, and SPK-organoids transplanted into the liver of C57BL/6 mice. Data are means ± SEM ($n = 4$ mice per group). (F) Gross appearance of the liver at 22 days after transplantation of normal, SP-, or SPK-organoids. Scale bar, 10 mm. (G) Summary of the incidence of liver tumors and lung metastases in C57BL/6 mice with orthotopically transplanted liver organoids. (H) Quantification of bioluminescence of normal, SP-, and SPK-organoids ($n = 3$, 4, and 3, respectively) transplanted into the liver of NSG mice. Data are means ± SEM. (I) Quantification of tumor volume for SP- and SPK-organoids injected s.c. into Balb/c-nu/nu mice. Data are means ± SEM ($n = 5$ mice per group). (J,K) Representative hematoxylin–eosin staining of the liver tumor (J) and lung metastases (K) that developed from SPK-organoids in a C57BL/6 mouse. Arrows indicate lung metastases. Scale bars, 500 μm (J) or 1 mm (K). (L) Staining of a liver tumor derived from SPK-organoids with picro-Sirius red. Scale bar, 100 μm. (M–O) Immunohistofluorescence staining of liver tumors derived from SPK-organoids expressing Venus-Akaluc with antibodies to Krt19 (M), to Sox9 (N), and to αSMA (O). Nuclei were stained with 4′,6-diamidino-2-phenylindole (DAPI). Scale bars, 50 μm.

allele for the *Kras*$^{G12D}$ mutation into SP-organoids with an sgRNA targeting exon 2 of *Kras* as well as a donor vector harboring *Kras*$^{G12D}$ and a synonymous protospacer adjacent motif (PAM) mutation flanked by ~500-bp homology arms. The *Kras*$^{G12D}$ mutant (SPK-) organoids selectively grew in medium lacking all MAPK-activating niche factors (HGF, EGF, FGF10, and gastrin) and containing gefitinib, a tyrosine kinase inhibitor of the EGF receptor, given the constitutive activation of Kras conferred by the G12D mutation (Figure 1D,E). This sequential mutagenesis and corresponding selection protocol thus allowed us to establish liver ductal organoids harboring the desired genetic alterations, as was confirmed by Sanger sequencing of the *Smad4*, *Trp53*, and *Kras* loci (Figure 1F–H).

### 3.2 | SPK-Organoids Form Primary Liver and Metastatic Tumors in Syngeneic Mice

To evaluate the tumorigenicity of normal, SP-, and SPK-organoids, we introduced a Venus-Akaluc fusion protein into these organoids by retroviral transduction (which allowed bioluminescence monitoring with the AkaBLI system) [25] and we then injected the modified organoids into the liver of WT C57BL/6 mice (Figure 2A). Monitoring of bioluminescence revealed that the normal organoids failed to engraft to the liver, and that, whereas the SP-organoids did manifest engraftment soon after transplantation, they were subsequently eliminated over time (Figure 2B,C,E). In contrast, transplantation of SPK-organoids resulted in marked and sustained tumor growth after engraftment (Figure 2D,E), leading to the formation of macroscopic tumors by 22 days after transplantation in all the recipient mice (Figure 2F,G,J). Similar findings were obtained for transplantation of the organoids into immunodeficient NOD.Cg-*Prkdc*$^{scid}$*Il2rg*$^{tm1Wjl}$/SzJ (NSG) mice (Figure 2H) and Balb/c-nu/nu mice (Figure 2I), suggesting that Smad4 and p53 inactivation promotes tumor initiation, and that additional Kras (G12D) mutation plays a key role in the sustained growth of CCA. Of note, some of the C57BL/6 mice transplanted with SPK-organoids showed lung metastasis (Figure 2G,K), suggesting that these three carcinogenic mutations are sufficient to recapitulate the invasive and metastatic features of human CCA. For primary liver tumors formed by SPK-organoids expressing Venus-Akaluc, immunohistofluorescence analysis revealed that Venus$^+$ cells expressed the bile duct markers cytokeratin 19 (Krt19) (Figure 2M) and Sox9 (Figure 2N) at a high level, and that these cells were surrounded by desmoplastic stroma (Figure 2L) and α-smooth muscle actin (αSMA)-positive cancer-associated fibroblasts (Figure 2O). These characteristics are consistent with those often observed for human CCA specimens [26]. Collectively, these results suggested that SPK-organoids are able to form CCA tumors in a syngeneic transplantation model that recapitulates both the clinical kinetics and histopathologic features of human CCA.

### 3.3 | SPK-Organoids Give Rise to a Tumor Immune Microenvironment Similar to That of Human CCA

We next investigated the tumor immune microenvironment within the primary tumors derived from SPK-organoids (Figure 3A). Flow cytometric analysis and immunohistofluorescence staining revealed a significant infiltration of CD45$^+$ leukocytes in tumors compared with adjacent normal liver tissue (Figure 3B,C), a finding reminiscent of human CCA tumors [3]. Detailed analysis of immune cell subsets within tumor and adjacent normal tissue showed that the numbers of Tregs, M2 macrophages, and neutrophils were increased, whereas the number of CD8$^+$ T cells was decreased, in tumor tissue (Figure 3D–L). These findings are consistent with those for the malignant form of human CCA, in which they are associated with poor overall and recurrence-free survival, postoperative distant metastasis, and chemotherapy resistance [3]. Together, our results indicated that SPK-organoid-derived tumors recapitulate the tumor immune microenvironment of human CCA.

### 3.4 | TINs Suppress CCA Tumor Growth

Given that Tregs, M2 macrophages, and neutrophils have been shown to play tumor-supportive roles in various cancer types [27, 28], we postulated that depletion of these cells might have a suppressive effect on CCA tumor growth. We first depleted Tregs with 67.9% efficiency by i.p. injection of antibodies targeting the Treg cell marker CD25 (Figure 4A,B), but such depletion had no significant effect on the growth of tumors formed by SPK-organoids in C57BL/6 mice (Figure 4C). To examine the effect



13497006, 2025, 9, Downloaded from https://onlinelibrary.wiley.com/doi/10.1111/cas.70129 by Tokyo Medical & Dental, Wiley Online Library on [06/10/2025]. See the Terms and Conditions (https://onlinelibrary.wiley.com/terms-and-conditions) on Wiley Online Library for rules of use; OA articles are governed by the applicable Creative Commons License

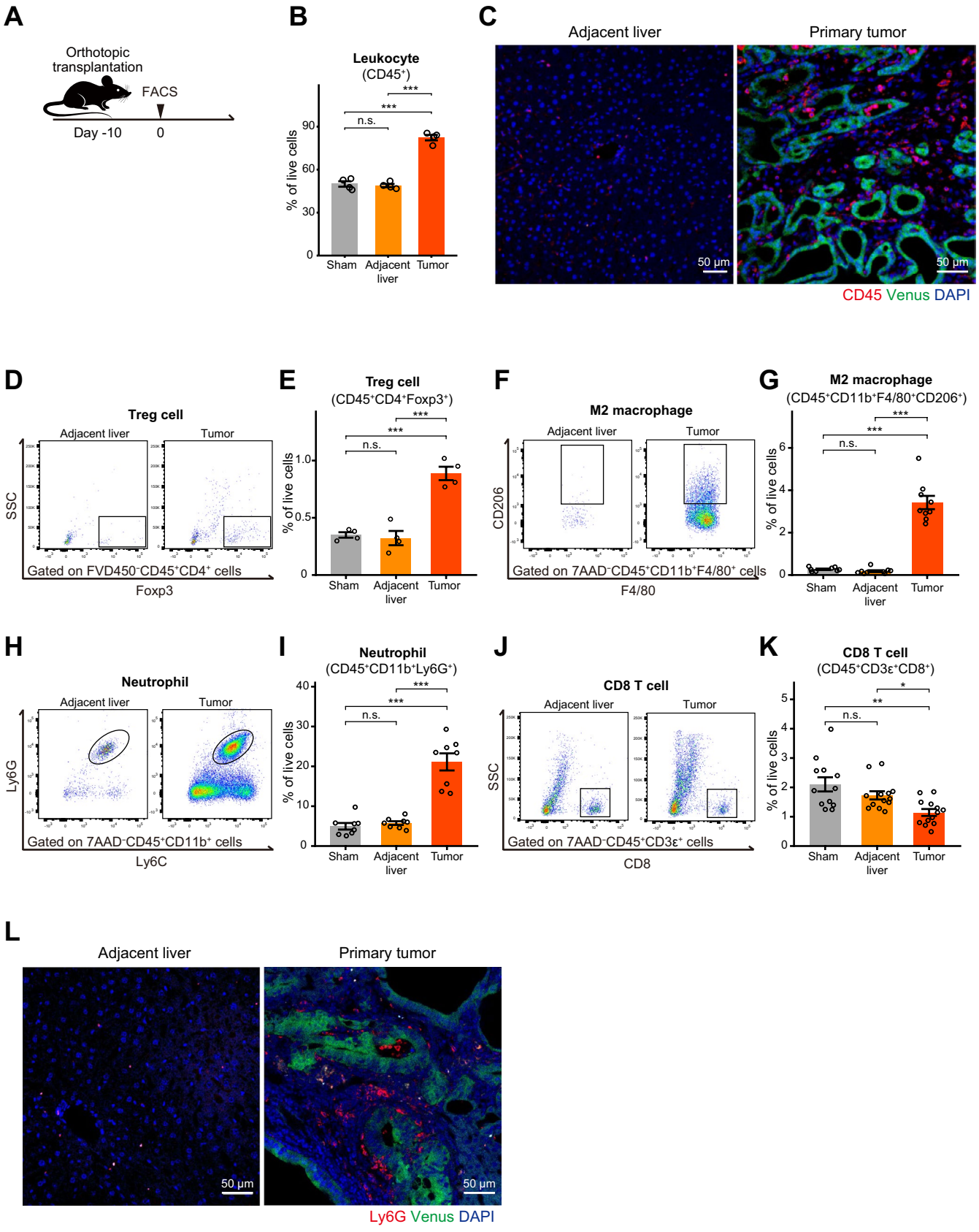



**FIGURE 3** | Legend on next page.



13497006, 2025, 9, Downloaded from https://onlinelibrary.wiley.com/doi/10.1111/cas.70129 by Tokyo Medical & Dental, Wiley Online Library on [06/10/2025]. See the Terms and Conditions (https://onlinelibrary.wiley.com/terms-and-conditions) on Wiley Online Library for rules of use; OA articles are governed by the applicable Creative Commons License

**FIGURE 3** | Orthotopically transplanted organoids recapitulate the inflammatory features of human CCA. (A) Schematic representation for analysis of the cellular composition of liver tumors. SPK-organoids expressing retrovirally transduced Venus-Akaluc protein were orthotopically transplanted into C57BL/6 mice on day −10 and analyzed on day 0. (B) Flow cytometric quantification of the percentage of $CD45^+$ leukocytes in sham-operated liver, tumor-adjacent liver tissue, and SPK-organoid–derived tumors. Data are means ± SEM ($n = 4$ mice per group). (C, L) Representative immunofluorescence staining of CD45 (C) and Ly6G (L) in tumor-adjacent liver and tumor tissue. Nuclei were stained with DAPI. Scale bars, 50 μm. (D, F, H, J) Representative flow cytometry plots for Tregs (D), M2 macrophages (F), neutrophils (H), and $CD8^+$ T cells (J) in tumor-adjacent liver and tumor tissue. SSC, side scatter. (E, G, I, K) Flow cytometric quantification of Tregs (E), M2 macrophages (G), neutrophils (I), and $CD8^+$ T cells (K) in sham-operated liver, tumor-adjacent liver tissue, and tumors. Data are means ± SEM ($n = 4$ to 13 mice per group). $^*p < 0.05$, $^{**}p < 0.01$, $^{***}p < 0.001$; n.s., not significant (Tukey–Kramer test).

of M2 macrophage depletion, we transplanted SPK-organoids into the liver of C-C chemokine receptor type 2 (CCR2)-deficient mice (Figure 4D). CCR2 is the receptor for C-C motif chemokine 2 (CCL2, also known as monocyte chemotaxis protein 1), and is essential for the exit of monocytes from bone marrow followed by their migration to target tissues and differentiation into tissue macrophages [29]. In tumors, these cells can transform into tumor-associated macrophages, which are polarized toward either an antitumor (M1) or a protumor (M2) phenotype depending on the tumor microenvironment [28]. Tumor-infiltrating monocytes and M2 macrophages were depleted in CCR2-deficient mice with an efficiency of 94.1% and 40.7%, respectively (Figure 4E,F), but such depletion again had no significant effect on tumor growth (Figure 4G). Finally, neutrophils were depleted in WT C57BL/6 mice by i.p. injection of antibodies to Ly6G combined with mouse antibodies to rat Igκ light chain that augment neutrophil elimination by anti-Ly6G treatment (Figure 4H) [30], resulting in an 82.5% and 63.1% reduction in the number of neutrophils in peripheral blood (Figure 4I) or tumors (Figure 4J), respectively. We found that such neutrophil depletion significantly accelerated CCA tumor growth compared with that apparent in mice treated with isotype control antibodies (Figure 4K), a finding opposite to that previously obtained for hepatocellular carcinoma [31]. Collectively, these data suggested that TINs function as a tumor-suppressive cell population in CCA.

### 3.5 | TINs Directly Kill Cancer Cells in a ROS-Dependent Manner

Given the unexpected antitumoral activity of neutrophils apparent in our syngeneic CCA model, we next focused on the characterization and manipulation of this neutrophil function. To investigate the mechanism underlying the antitumoral effect of TINs, we isolated these cells by fluorescence-activated cell sorting (FACS) and cultured them with adherent SPK-cells expressing Akaluc (Figure 5A). This killing assay revealed a cell number-dependent cytotoxicity of neutrophils, with the results suggesting direct killing rather than induction of cell cycle arrest in the tumor cells (Figures 5B, S1). Neutrophils produce large amounts of ROS as a result of the activation of the NADPH oxidase complex (Figure 5C), and they thereby exert an antimicrobial function against phagocytosed pathogens [32]. Given that neutrophils are also capable of damaging neighboring cancer cells through extracellular ROS release [33, 34], we tested the effect of ROS removal on neutrophil cytotoxicity for CCA with the use of several antioxidants. The cytotoxic activity of neutrophils against SPK-cells was abrogated in the presence of superoxide dismutase (SOD) or catalase—both of which mediate the enzymatic degradation of ROS—or of taurine, which serves as a hypochlorous acid scavenger (Figure 5D). Together, these results suggested that TINs directly damage CCA cells in a manner dependent on ROS production.

### 3.6 | G-CSF Increases the Number of TINs and the Survival of Tumor-Bearing Mice

Given that neutrophil production is largely under the control of G-CSF, a cytokine that stimulates the proliferation of granulocyte progenitors and facilitates their differentiation into mature neutrophils [35, 36], we speculated that G-CSF might play an important role in CCA progression through the regulation of TINs. Kaplan–Meier analysis of gene expression and prognostic data for human CCA patients indeed showed that individuals with a higher tumor expression level of the G-CSF gene (*CSF3*) had a longer overall survival (Figure 6A), suggestive of a tumor-suppressive function for G-CSF. To investigate directly the impact of G-CSF on TINs and tumor growth in CCA, we generated G-CSF-deficient mice that harbor an 8-bp deletion in exon 2 of *Csf3* on both alleles (Figure 6B) and which manifest chronic and steady-state neutropenia (Figure 6C), consistent with previous observations [35]. G-CSF-deficient mice orthotopically transplanted with SPK-organoids showed a reduced number of TINs (Figure 6D,E) as well as a significantly increased tumor volume (Figure 6F) and shortened survival (Figure 6G) compared with their WT counterparts. Given that rhG-CSF is commonly administered in clinical practice, we next examined the therapeutic potential of rhG-CSF for CCA. In contrast to the results obtained with G-CSF-deficient mice, daily administration of rhG-CSF to WT mice transplanted with SPK-organoids resulted in an increase in the number of TINs (Figure 6H,I), suppression of tumor growth (Figure 6J), and prolonged recipient survival (Figure 6K). Collectively, these findings suggested that G-CSF serves as a protective factor against CCA progression by regulating TIN counts, highlighting the possibility of rhG-CSF administration as a novel therapeutic option for CCA.

### 3.7 | rhG-CSF Administration Shows a Synergistic Effect With Standard Chemotherapy for CCA

To investigate further the mechanism responsible for the tumor-suppressive effect of rhG-CSF administration, we isolated TINs from control and rhG-CSF-treated CCA-bearing mice by FACS



13497006, 2025, 9, Downloaded from https://onlinelibrary.wiley.com/doi/10.1111/cas.70129 by Tokyo Medical & Dental, Wiley Online Library on [06/10/2025]. See the Terms and Conditions (https://onlinelibrary.wiley.com/terms-and-conditions) on Wiley Online Library for rules of use; OA articles are governed by the applicable Creative Commons License

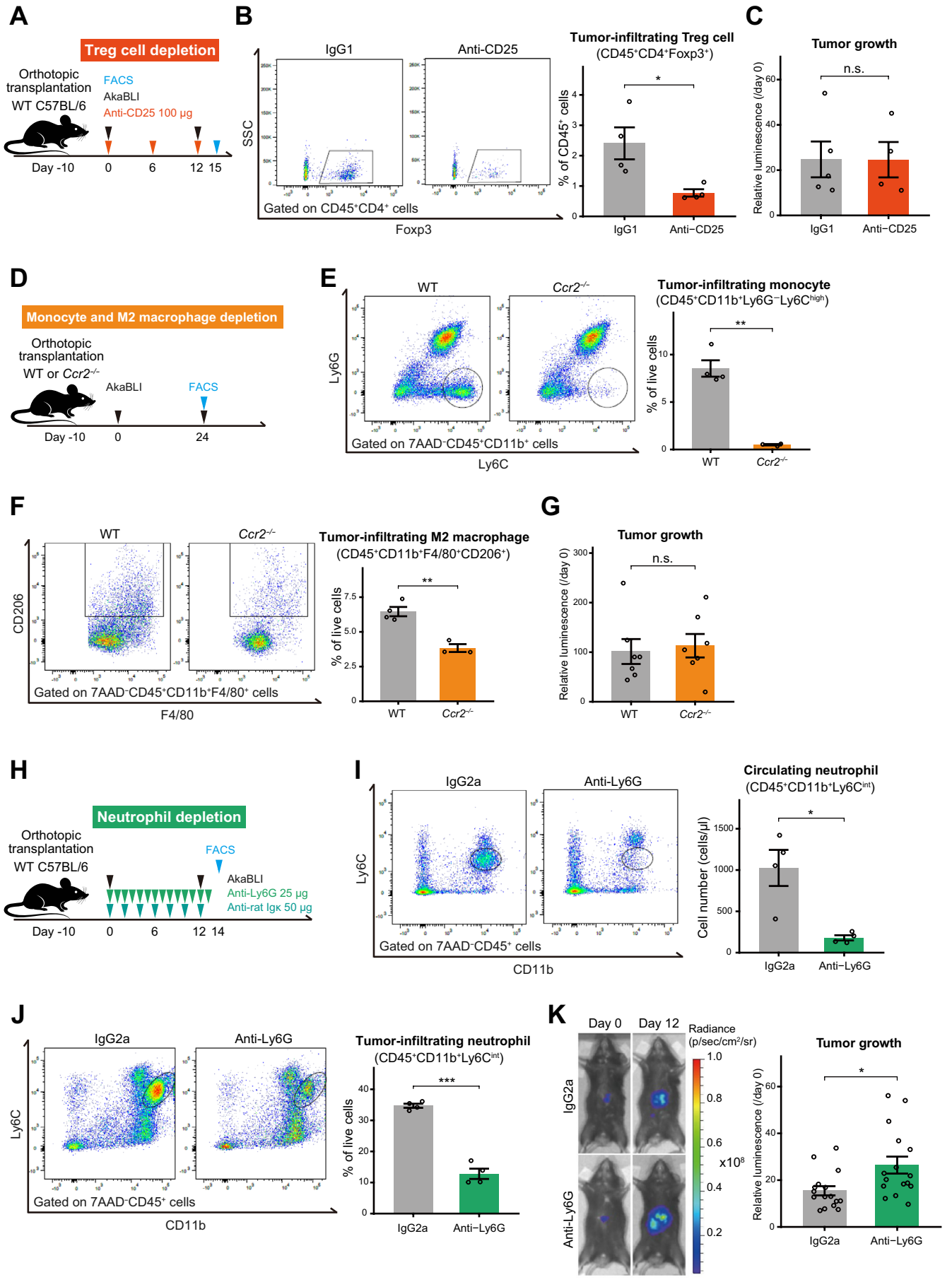



**FIGURE 4** | Legend on next page.



13497006, 2025, 9, Downloaded from https://onlinelibrary.wiley.com/doi/10.1111/cas.70129 by Tokyo Medical & Dental, Wiley Online Library on [06/10/2025]. See the Terms and Conditions (https://onlinelibrary.wiley.com/terms-and-conditions) on Wiley Online Library for rules of use; OA articles are governed by the applicable Creative Commons License

**FIGURE 4** | Selective depletion of tumor-infiltrating immune cells reveals an antitumor action of neutrophils. (A–C) WT C57BL/6 mice were orthotopically transplanted with Venus-Akaluc–expressing SPK-organoids on day −10 and treated with control IgG1 or antibodies to CD25 on days 0, 6, and 12 (A). Representative flow cytometry plots and quantification of intratumoral Tregs on day 15 for tumor-bearing mice treated with control IgG1 ($n=4$) or anti-CD25 ($n=4$) (B). Relative bioluminescence of liver tumors on day 12 for mice treated with control IgG1 ($n=5$) or anti-CD25 ($n=4$) (C). (D–G) Venus-Akaluc–expressing SPK-organoids were orthotopically transplanted in WT or *Ccr2*$^{-}$ mice (D). Representative flow cytometry plots and quantification of monocytes isolated from tumors of WT ($n=4$) or *Ccr2*$^{-}$ ($n=3$) mice on day 24 (E). Representative flow cytometry plots and quantification of M2 macrophages isolated from tumors of WT ($n=4$) or *Ccr2*$^{-}$ ($n=3$) mice on day 24 (F). Relative bioluminescence of liver tumors on day 24 in WT ($n=7$) and *Ccr2*$^{-}$ ($n=7$) mice (G). (H–K) WT C57BL/6 mice were orthotopically transplanted with Venus-Akaluc–expressing SPK-organoids and treated with antibodies to rat Igκ light chain and either control IgG2a or antibodies to Ly6G. Control IgG2a and anti-Ly6G were administered daily, whereas anti-rat Igκ light chain was administered every 2 days (H). Representative flow cytometry plots and quantification of circulating neutrophils on day 6 for tumor-bearing mice treated with control IgG2a ($n=4$) or anti-Ly6G ($n=4$) (I). Representative flow cytometry plots and quantification of TINs on day 14 for tumor-bearing mice treated with control IgG2a ($n=4$) or anti-Ly6G ($n=4$) (J). Relative bioluminescence of liver tumors on day 12 in mice treated with control IgG2a ($n=16$) or anti-Ly6G ($n=16$) (K). Quantitative data in bar graphs are means ± SEM. *$p<0.05$, **$p<0.01$, ***$p<0.001$; n.s., not significant (Welch's *t* test).

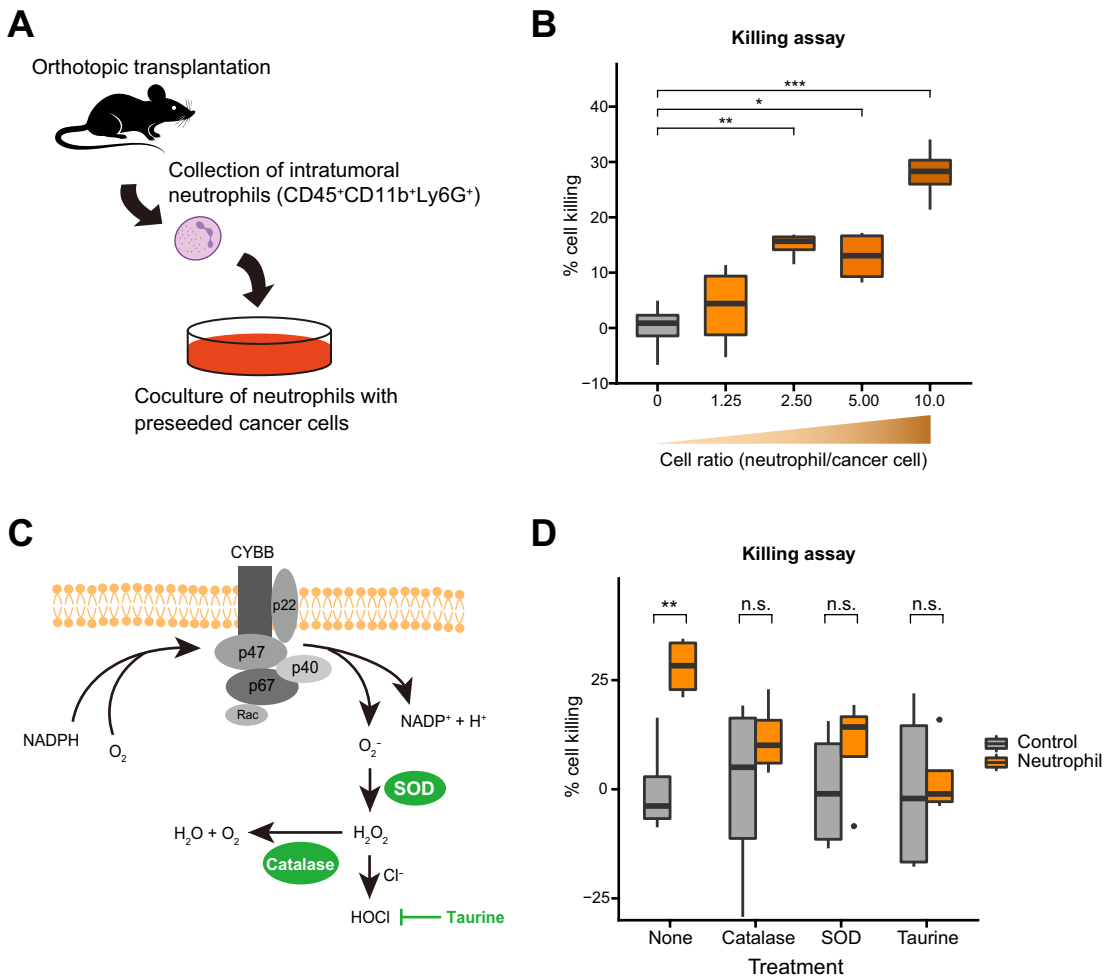



**FIGURE 5** | Cytotoxicity of TINs for CCA is mediated by ROS. (A) Experimental protocol for assessment of neutrophil cytotoxicity. TINs were isolated by FACS from tumors formed by SPK-organoids in C57BL/6 mice and were cultured with preseeded Venus-Akaluc-expressing SPK-cancer cells in adherent culture. (B) Quantification of cytotoxicity as in (A) with a fixed number of cancer cells and various numbers of TINs. Data are presented as box-and-whisker plots, with the boxes indicating quartile values and the whiskers denoting the range of the data, excluding outliers ($n=4$ independent experiments). (C) Production of ROS by the NADPH oxidase complex. SOD converts superoxide to $H_2O_2$, catalase catalyzes the degradation of $H_2O_2$ to $H_2O$ and $O_2$, and taurine eliminates HOCl. (D) Quantification of TIN cytotoxicity as in (A) in the absence or presence of catalase, SOD, or taurine ($n=4$ independent experiments). *$p<0.05$, **$p<0.01$, ***$p<0.001$; n.s., not significant by Dunnett's test (B) or Welch's *t* test (D).



13497006, 2025, 9, Downloaded from https://onlinelibrary.wiley.com/doi/10.1111/cas.70129 by Tokyo Medical & Dental, Wiley Online Library on [06/10/2025]. See the Terms and Conditions (https://onlinelibrary.wiley.com/terms-and-conditions) on Wiley Online Library for rules of use; OA articles are governed by the applicable Creative Commons License

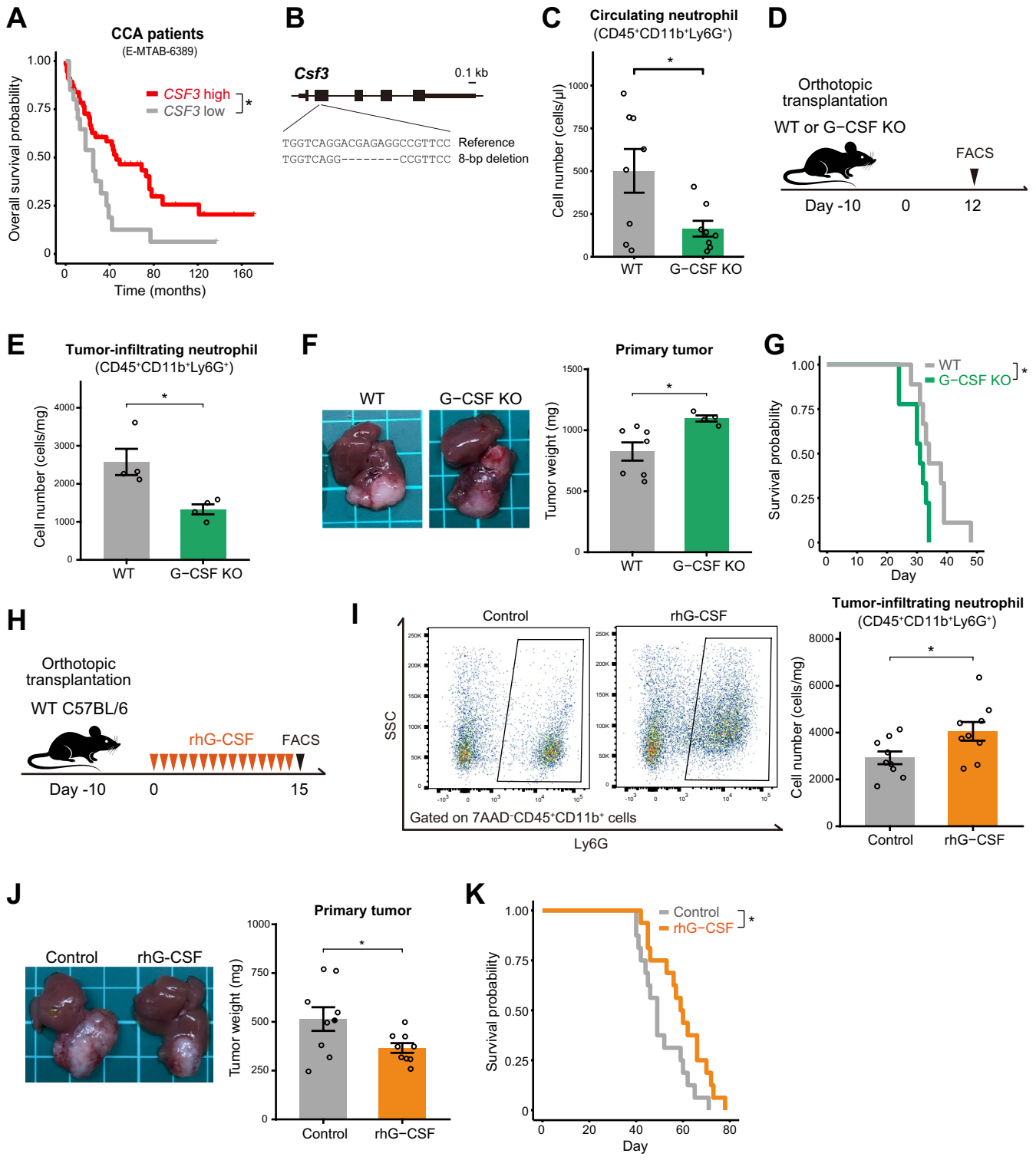



**FIGURE 6** | Legend on next page.

and subjected them to scRNA-seq analysis. Clustering and *t*-distributed stochastic neighbor embedding (*t*-SNE) analysis revealed that rhG-CSF-stimulated and control TINs were classified into almost completely distinct populations (Figure 7A). Given that neutrophils have been shown to be a heterogeneous population composed of immature and mature cells, which have been associated with protumor and antitumor activity [15], respectively, we assessed the effect of rhG-CSF treatment on the TIN differentiation level with the use of CytoTRACE, an algorithm for prediction of cell maturity on the basis of the correlation between cell differentiation states and the number of expressed genes [37]. CytoTRACE analysis revealed that rhG-CSF-stimulated TINs were more differentiated compared with control TINs (Figure 7B), suggesting that rhG-CSF treatment



13497006, 2025, 9, Downloaded from https://onlinelibrary.wiley.com/doi/10.1111/cas.70129 by Tokyo Medical & Dental, Wiley Online Library on [06/10/2025]. See the Terms and Conditions (https://onlinelibrary.wiley.com/terms-and-conditions) on Wiley Online Library for rules of use; OA articles are governed by the applicable Creative Commons License

**FIGURE 6** | Therapeutic effect of rhG-CSF administration in CCA-bearing mice. (A) Overall survival curves for CCA patients in the E-MTAB-6389 data set with high ($n=56$) or low ($n=20$) levels of *CSF3* expression. (B) G-CSF-deficient mice were generated by introduction of an 8-bp deletion in exon 2 of both alleles of the *Csf3* gene. (C) Flow cytometric quantification of peripheral blood neutrophils in WT and G-CSF knockout (KO) mice. Data are means ± SEM ($n=8$ mice per group). (D–G) SPK-organoids were orthotopically transplanted in WT mice or G-CSF KO mice on day −10, and the mice were analyzed on day 12 (D). Flow cytometric quantification of TINs on day 12 in WT ($n=4$) and G-CSF KO ($n=4$) mice; data are means ± SEM (E). Gross appearance of liver tumors and quantification of tumor weight on day 12 in WT ($n=7$) and G-CSF KO ($n=4$) mice; data are means ± SEM (F). Survival curves for WT ($n=9$) and G-CSF KO ($n=9$) mice with orthotopically transplanted SPK-organoids (G). (H–K) WT C57BL/6 mice were orthotopically transplanted with SPK-organoids on day −10 and were injected s.c. with rhG-CSF or phosphate-buffered saline (PBS) daily for 15 days beginning on day 0 (H). Representative flow cytometry plots and quantification of TINs on day 15 in tumor-bearing mice treated with PBS ($n=9$) or rhG-CSF ($n=9$); data are means ± SEM (I). Gross appearance of liver tumors and quantification of tumor weight on day 15 in mice treated with PBS ($n=9$) or rhG-CSF ($n=9$); data are means ± SEM (J). Survival curves for tumor-bearing mice treated with PBS ($n=16$) or rhG-CSF ($n=16$) (K). *$p<0.05$ by the log-rank test (A, G, K) or Welch's *t* test (C, E, F, I, J).

promoted the functional maturation of TINs. Furthermore, gene ontology (GO) term analysis revealed that genes associated with cell killing, ROS metabolism, and immune activation were upregulated in rhG-CSF-treated TINs (Figure 7C,D). Consistent with these results, culture of TINs with adherent SPK-cells revealed that prior exposure to rhG-CSF in vivo increased the cytotoxicity of the isolated TINs (Figure 7E). Finally, to examine the potential synergism of rhG-CSF administration with standard chemotherapy for treatment of CCA, we treated CCA-bearing mice with rhG-CSF in combination with gemcitabine and cisplatin (Figure 7F). Administration of rhG-CSF increased the number of TINs (Figure 7G) as well as significantly suppressed CCA tumor growth (Figure 7H) in mice receiving chemotherapy. Collectively, these results suggested that rhG-CSF administration augments the antitumoral function of TINs and thereby exerts a synergistic effect with standard chemotherapy on tumor growth.

## 4 | Discussion

We have here established a genetically defined and transplantable CCA model with the use of CRISPR/Cas9-mediated genome editing to introduce *Smad4*, *Trp53*, and *Kras* mutations into normal liver ductal organoids. The resulting SPK-organoids, when transplanted into immunocompetent mice, formed invasive and metastatic tumors that resembled human CCA. Our findings revealed that TINs exert antitumor activity dependent on ROS production. Furthermore, the administration of rhG-CSF increased the number and cytotoxicity of TINs, resulting in suppression of tumor growth and prolongation of survival in tumor-bearing mice. The combination of rhG-CSF and standard chemotherapy showed a synergistic effect on tumor growth that was significantly greater than that of rhG-CSF or chemotherapy alone.

In contrast to previous findings that neutrophils are primarily protumorigenic in CCA [16–18], our study revealed an antitumor activity of TINs in a genetically defined and immunocompetent CCA model. Several factors might explain this apparent discrepancy. First, the phenotype of the tumor immune microenvironment has been found to vary with cancer genotype in CCA [9]. The genetic profile of our CCA model differs from that of those in earlier studies [16–18], which may account for the observed difference in TIN phenotype. In addition, we studied an immunocompetent model rather than the immunodeficient mice studied previously [16–18], which might have affected the interplay between cancer cells and stromal cells. Finally, whereas the previous studies were primarily based on cell lines [16–18], we adopted a genetically defined organoid model, which may provide a more accurate representation of the tumor microenvironment.

Previous studies have shown the benefits of combining rhG-CSF with chemotherapy for various tumor types [38]. Such combination therapy reduces the risk of neutropenic complications associated with chemotherapy, resulting in improved disease control and survival as a consequence of minimization of chemotherapy dose reduction and treatment delay. Our study builds on this foundation by showing that the combination of rhG-CSF and standard chemotherapy not only leverages these general benefits but also enhances the antitumor activity of TINs in CCA. We found that rhG-CSF administration increased both the quantity and quality of TINs, which in turn contributed to the suppression of tumor growth and an improved survival rate in our CCA model. These results suggest that the modulation of neutrophil activity by rhG-CSF is a key factor in the therapeutic synergy with chemotherapy.

Despite its promising findings, our study has several limitations. First, although mouse models provide valuable insight into CCA, they may not fully recapitulate the complexity of the human disease. The genetic and immunologic differences between mice and humans may affect the translatability of results obtained from such models. Second, whereas CCA manifests diverse genetic profiles, our study mimicked only a subset of genetic alteration patterns. The properties of TINs might differ according to CCA genotype, potentially affecting the generalizability of our findings. Third, Venus-Akaluc expression in organoid cells and Matrigel use for organoid transplantation may also affect the tumor immune microenvironment. Lastly, our study did not investigate the potential interactions between TINs and other stromal cells within the tumor microenvironment, with characterization of such interactions being likely to provide a more comprehensive understanding of the CCA microenvironment.

In conclusion, our study provides a novel and genetically defined model for investigations of CCA and highlights the therapeutic potential of targeting TINs with rhG-CSF. Our findings underscore the importance of the tumor immune microenvironment in cancer progression and treatment, paving the way for innovative approaches to combat CCA.



13497006, 2025, 9, Downloaded from https://onlinelibrary.wiley.com/doi/10.1111/cas.70129 by Tokyo Medical & Dental, Wiley Online Library on [06/10/2025]. See the Terms and Conditions (https://onlinelibrary.wiley.com/terms-and-conditions) on Wiley Online Library for rules of use; OA articles are governed by the applicable Creative Commons License

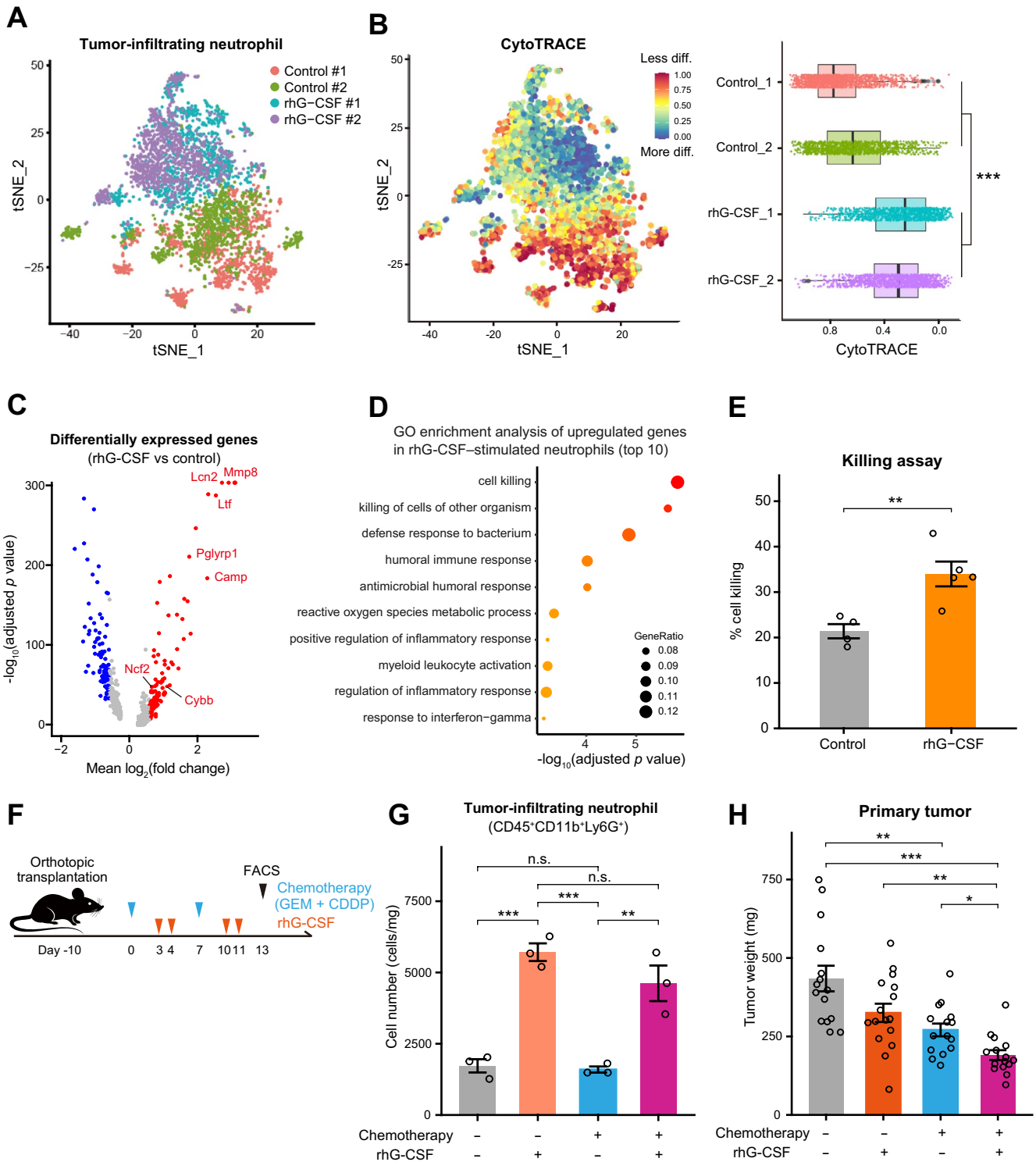



**FIGURE 7** | Administration of rhG-CSF enhances the cytotoxicity of TINs for CCA. (A) *t*-SNE projection of scRNA-seq data for TINs isolated from liver tumors formed by SPK-organoids in C57BL/6 mice and treated with PBS ($n=2$) or rhG-CSF ($n=2$) as in Figure 6H. (B) Heat map for CytoTRACE scores of the scRNA-seq data overlaid on the *t*-SNE map (left) and box plots showing CytoTRACE values for each treatment (right). Diff., differentiated. (C) Volcano plot showing differentially expressed genes (DEGs) for TINs from rhG-CSF-treated mice compared with those from control mice. (D) GO analysis of DEGs upregulated (fold change of $>1.5$ and adjusted *p* value of $<0.05$) for TINs from mice treated with rhG-CSF in (C). The top 10 terms for biological processes are shown. (E) Quantification of cytotoxicity toward adherent SPK-cells for TINs isolated from mice treated with PBS or rhG-CSF ($n=4$ or 5 independent experiments, respectively). (F–H) WT C57BL/6 mice were orthotopically transplanted with SPK-organoids and treated with gemcitabine (GEM), cisplatin (CDDP), and rhG-CSF. GEM and CDDP were administered i.p. on days 0 and 7, and rhG-CSF was administered s.c. on days 3, 4, 10, and 11 (F). Quantitation of TINs on day 13 for tumor-bearing mice treated with chemotherapy or rhG-CSF as indicated ($n=3$ mice per group) (G). Quantification of tumor weight on day 13 for mice treated with chemotherapy or rhG-CSF as indicated ($n=15$ to 16 mice per group) (H). Data in (E), (G), and (H) are means ± SEM. $^{*}p<0.05$, $^{**}p<0.01$, $^{***}p<0.001$; n.s., not significant by the Steel-Dwass test (B, H), Welch's *t* test (E), or the Tukey–Kramer test (G).



13497006, 2025, 9, Downloaded from https://onlinelibrary.wiley.com/doi/10.1111/cas.70129 by Tokyo Medical & Dental, Wiley Online Library on [06/10/2025]. See the Terms and Conditions (https://onlinelibrary.wiley.com/terms-and-conditions) on Wiley Online Library for rules of use; OA articles are governed by the applicable Creative Commons License

### Author Contributions

**Osamu Sugahara:** conceptualization, data curation, formal analysis, investigation, methodology, resources, validation, visualization, writing – original draft. **Daisuke Koga:** investigation, methodology. **Takeru Oka:** formal analysis, investigation. **Shigeaki Sugiyama:** formal analysis, investigation. **Reona Wada:** formal analysis, investigation. **Tsunaki Higa:** conceptualization, data curation, funding acquisition, supervision, writing – original draft. **Keiichi I. Nakayama:** conceptualization, funding acquisition, project administration, supervision, writing – original draft, writing – review and editing.


### Acknowledgments

We thank H. Takayoshi for technical assistance. Computations were performed in part on the NIG supercomputer at ROIS National Institute of Genetics.


### Ethics Statement

The study complies with all relevant ethics regulations. All mouse experiments were approved by the Animal Ethics Committees of Kyushu University (approval code A22-214-0) and Institute of Science Tokyo (approval code A2023-225A), and all experiments involving genetic manipulation were approved by the Safety Committees for Recombinant DNA Experiments of Kyushu University (approval code 30–38) and Institute of Science Tokyo (approval code G2023-087C).

### Consent

The authors have nothing to report.

### Conflicts of Interest

Keiichi I. Nakayama is an editorial board member of *Cancer Science* and receives annual profit from shares from AntiCancer Technologies Inc. and Q-Innovation Inc. Other authors do not have COI.

### References


1. J. M. Banales, J. J. G. Marin, A. Lamarca, et al., "Cholangiocarcinoma 2020: The Next Horizon in Mechanisms and Management," *Nature Reviews. Gastroenterology & Hepatology* 17 (2020): 557–588, https://doi.org/10.1038/s41575-020-0310-z.

2. H. Rumgay, M. Arnold, J. Ferlay, et al., "Global Burden of Primary Liver Cancer in 2020 and Predictions to 2040," *Journal of Hepatology* 77 (2022): 1598–1606, https://doi.org/10.1016/j.jhep.2022.08.021.

3. Y. Kitano, H. Okabe, Y. I. Yamashita, et al., "Tumour-Infiltrating Inflammatory and Immune Cells in Patients With Extrahepatic Cholangiocarcinoma," *British Journal of Cancer* 118 (2018): 171–180, https://doi.org/10.1038/bjc.2017.401.

4. M. A. Lowery, R. Ptashkin, E. Jordan, et al., "Comprehensive Molecular Profiling of Intrahepatic and Extrahepatic Cholangiocarcinomas: Potential Targets for Intervention," *Clinical Cancer Research* 24 (2018): 4154–4161, https://doi.org/10.1158/1078-0432.CCR-18-0078.

5. A. Lamarca, J. Barriuso, M. G. McNamara, and J. W. Valle, "Molecular Targeted Therapies: Ready for "Prime Time" in Biliary Tract Cancer," *Journal of Hepatology* 73 (2020): 170–185, https://doi.org/10.1016/j.jhep.

6. G. Jiang, W. Zhang, T. Wang, et al., "Characteristics of Genomic Alterations in Chinese Cholangiocarcinoma Patients," *Japanese Journal of Clinical Oncology* 50 (2020): 1117–1125, https://doi.org/10.1093/jjco/hyaa088.

7. J. G. Yoon, M. H. Kim, M. Jang, et al., "Molecular Characterization of Biliary Tract Cancer Predicts Chemotherapy and Programmed Death 1/Programmed Death-Ligand 1 Blockade Responses," *Hepatology* 74 (2021): 1914–1931, https://doi.org/10.1002/hep.31862.

8. G. Kendre, K. Murugesan, T. Brummer, O. Segatto, A. Saborowski, and A. Vogel, "Charting Co-Mutation Patterns Associated With Actionable Drivers in Intrahepatic Cholangiocarcinoma," *Journal of Hepatology* 78 (2023): 614–626, https://doi.org/10.1016/j.jhep.2022.11.030.

9. J. L. Tomlinson, B. Li, J. Yang, et al., "Syngeneic Murine Models With Distinct Immune Microenvironments Represent Subsets of Human Intrahepatic Cholangiocarcinoma," *Journal of Hepatology* 80 (2024): 892–903, https://doi.org/10.1016/j.jhep.2024.02.008.

10. B. A. William, W. Wenjia, A. H. Margaret, et al., "Smad4 Restricts Injury-Provoked Biliary Proliferation and Carcinogenesis," *Disease Models & Mechanisms* 17, no. 6 (2024): dmm050358, https://doi.org/10.1242/dmm.050358.

11. E. J. C. A. Kamp, W. N. M. Dinjens, M. Doukas, et al., "Genetic Alterations During the Neoplastic Cascade Towards Cholangiocarcinoma in Primary Sclerosing Cholangitis," *Journal of Pathology* 258 (2022): 227–235, https://doi.org/10.1002/path.5994.

12. S. Y. Cho, H. Hwang, Y. H. Kim, et al., "Refining Classification of Cholangiocarcinoma Subtypes via Proteogenomic Integration Reveals New Therapeutic Prospects," *Gastroenterology* 164 (2023): 1293–1309, https://doi.org/10.1053/j.gastro.2023.02.045.

13. S. Jaillon, A. Ponzetta, D. Di Mitri, A. Santoni, R. Bonecchi, and A. Mantovani, "Neutrophil Diversity and Plasticity in Tumour Progression and Therapy," *Nature Reviews. Cancer* 20 (2020): 485–503, https://doi.org/10.1038/s41568-020-0281-y.

14. L. G. Ng, R. Ostuni, and A. Hidalgo, "Heterogeneity of Neutrophils," *Nature Reviews. Immunology* 19 (2019): 255–265, https://doi.org/10.1038/s41577-019-0141-8.

15. C. C. Hedrick and I. Malanchi, "Neutrophils in Cancer: Heterogeneous and Multifaceted," *Nature Reviews. Immunology* 22 (2022): 173–187, https://doi.org/10.1038/s41577-021-00571-6.

16. S. L. Zhou, Z. Dai, Z. J. Zhou, et al., "CXCL5 Contributes to Tumor Metastasis and Recurrence of Intrahepatic Cholangiocarcinoma by Recruiting Infiltrative Intratumoral Neutrophils," *Carcinogenesis* 35 (2014): 597–605, https://doi.org/10.1093/carcin/bgt397.

17. M. Yoshimoto, S. Kagawa, H. Kajioka, et al., "Dual Antiplatelet Therapy Inhibits Neutrophil Extracellular Traps to Reduce Liver Micrometastases of Intrahepatic Cholangiocarcinoma," *Cancer Letters* 567 (2023), https://doi.org/10.1016/j.canlet.2023.216260.

18. Z. Zhou, P. Wang, R. Sun, et al., "Tumor-Associated Neutrophils and Macrophages Interaction Contributes to Intrahepatic Cholangiocarcinoma Progression by Activating STAT3," *Journal for Immunotherapy of Cancer* 9 (2021): 9, https://doi.org/10.1136/jitc-2020-001946.

19. Z. Zhao, X. Chen, A. M. Dowbaj, et al., "Organoids," *Nature Reviews Methods Primers* 2 (2022), https://doi.org/10.1038/s43586-022-00174-y.

20. M. Matano, S. Date, M. Shimokawa, et al., "Modeling Colorectal Cancer Using CRISPR-Cas9-Mediated Engineering of Human Intestinal Organoids," *Nature Medicine* 21 (2015): 256–262, https://doi.org/10.1038/nm.3802.

21. T. Seino, S. Kawasaki, M. Shimokawa, et al., "Human Pancreatic Tumor Organoids Reveal Loss of Stem Cell Niche Factor Dependence During Disease Progression," *Cell Stem Cell* 22 (2018): 454–467.e6, https://doi.org/10.1016/j.stem.2017.12.009.

22. J. Kim, B. K. Koo, and J. A. Knoblich, "Human Organoids: Model Systems for Human Biology and Medicine," *Nature Reviews. Molecular Cell Biology* 21 (2020): 571–584, https://doi.org/10.1038/s41580-020-0259-3.

23. J. Le Dai, R. K. Bansal, and S. E. Kern, "G 1 Cell Cycle Arrest and Apoptosis Induction by Nuclear Smad4Dpc4: Phenotypes Reversed by a Tumorigenic Mutation," *Proceedings of the National Academy of Sciences of the United States of America* 96, no. 4 (1999): 1427–1432.




13497006, 2025, 9, Downloaded from https://onlinelibrary.wiley.com/doi/10.1111/cas.70129 by Tokyo Medical & Dental, Wiley Online Library on [06/10/2025]. See the Terms and Conditions (https://onlinelibrary.wiley.com/terms-and-conditions) on Wiley Online Library for rules of use; OA articles are governed by the applicable Creative Commons License

24. B. Schmierer and C. S. Hill, "TGFβ-SMAD Signal Transduction: Molecular Specificity and Functional Flexibility," *Nature Reviews. Molecular Cell Biology* 8 (2007): 970–982, https://doi.org/10.1038/nrm2297.

25. S. Iwano, M. Sugiyama, H. Hama, et al., "Single-Cell Bioluminescence Imaging of Deep Tissue in Freely Moving Animals," *Science* 359, no. 6378 (2018): 935–939.

26. N. Guedj, L. Blaise, F. Cauchy, M. Albuquerque, O. Soubrane, and V. Paradis, "Prognostic Value of Desmoplastic Stroma in Intrahepatic Cholangiocarcinoma," *Modern Pathology* 34 (2021): 408–416, https://doi.org/10.1038/s41379-020-00656-y.

27. J. L. Tomlinson, J. W. Valle, and S. I. Ilyas, "Immunobiology of Cholangiocarcinoma," *Journal of Hepatology* 79 (2023): 867–875, https://doi.org/10.1016/j.jhep.2023.05.010.

28. K. E. de Visser and J. A. Joyce, "The Evolving Tumor Microenvironment: From Cancer Initiation to Metastatic Outgrowth," *Cancer Cell* 41 (2023): 374–403, https://doi.org/10.1016/j.ccell.2023.02.016.

29. L. Fei, X. Ren, H. Yu, and Y. Zhan, "Targeting the CCL2/CCR2 Axis in Cancer Immunotherapy: One Stone, Three Birds?," *Frontiers in Immunology* 12 (2021), https://doi.org/10.3389/fimmu.2021.771210.

30. G. Boivin, J. Faget, P. B. Ancey, et al., "Durable and Controlled Depletion of Neutrophils in Mice," *Nature Communications* 11 (2020), https://doi.org/10.1038/s41467-020-16596-9.

31. R. Xue, Q. Zhang, Q. Cao, et al., "Liver Tumour Immune Microenvironment Subtypes and Neutrophil Heterogeneity," *Nature* 612 (2022): 141–147, https://doi.org/10.1038/s41586-022-05400-x.

32. T. Németh, M. Sperandio, and A. Mócsai, "Neutrophils as Emerging Therapeutic Targets," *Nature Reviews. Drug Discovery* 19 (2020): 253–275, https://doi.org/10.1038/s41573-019-0054-z.

33. Z. Granot, E. Henke, E. A. Comen, T. A. King, L. Norton, and R. Benezra, "Tumor Entrained Neutrophils Inhibit Seeding in the Premetastatic Lung," *Cancer Cell* 20 (2011): 300–314, https://doi.org/10.1016/j.ccr.2011.08.012.

34. J. Yan, G. Kloecker, C. Fleming, et al., "Human Polymorphonuclear Neutrophils Specifically Recognize and Kill Cancerous Cells," *Oncoimmunology* 3 (2014): e950163, https://doi.org/10.4161/15384101.2014.950163.

35. G. J. Lieschke, D. Grail, G. Hodgson, et al., "Mice Lacking Granulocyte Colony-Stimulating Factor Have Chronic Neutropenia, Granulocyte and Macrophage Progenitor Cell Deficiency, and Impaired Neutrophil Mobilization," *Blood* 84, no. 6 (1994): 1737–1746.

36. F. Liu, Y. Wu, and R. Wesselschmidt, "Impaired Production and Increased Apoptosis of Neutrophils in Granulocyte Colony-Stimulating Factor Receptor-Deficient Mice," *Immunity* 5, no. 5 (1996): 491–501.

37. G. S. Gulati, S. S. Sikandar, D. J. Wesche, et al., "Single-Cell Transcriptional Diversity Is a Hallmark of Developmental Potential," *Science* 367, no. 6476 (2020): 405–411.

38. G. H. Lyman, L. Yau, R. Nakov, and A. Krendyukov, "Overall Survival and Risk of Second Malignancies With Cancer Chemotherapy and G-CSF Support," *Annals of Oncology* 29 (2018): 1903–1910, https://doi.org/10.1093/annonc/mdy311.

**Supporting Information**

Additional supporting information can be found online in the Supporting Information section.



13497006, 2025, 9, Downloaded from https://onlinelibrary.wiley.com/doi/10.1111/cas.70129 by Tokyo Medical & Dental, Wiley Online Library on [06/10/2025]. See the Terms and Conditions (https://onlinelibrary.wiley.com/terms-and-conditions) on Wiley Online Library for rules of use; OA articles are governed by the applicable Creative Commons License